Light Metals 2012 *Edited by: Carlos E. Suarez*
TMS (The Minerals, Metals & Materials Society), 2012

Light Metals 2012

ALUMINUM ALLOYS: Fabrication, Characterization and Applications

Thermal Mechanical Processing

SESSION CHAIR
Xiyu Wen
University of Kentucky
Lexington, Kentucky, USA

Light Metals 2012 *Edited by: Carlos E. Suarez*
TMS (The Minerals, Metals & Materials Society), 2012

Modeling of as-cast A356 for coupled explicit finite element analysis

M. J. Roy[1] and D. M. Maijer[1]

[1]Department of Materials Engineering, The University of British Columbia, 309-6350 Stores Road, Vancouver, BC V6T 1Z4, Canada

Keywords: A356, explicit, finite element, constitutive behaviour

Abstract

Design tools to simulate the manufacturing processes applied to aluminum components require computationally efficient finite element methods. While static processes such as casting employ implicit techniques, dynamic processes such as forging may only be modeled with explicitly. A commonplace practice to expedite explicit simulations is to employ time or mass scaling, which can lead to unexpected thermal-mechanical behaviour in coupled analyses. In both cases, the development of fully coupled thermo-mechanical simulations necessitates the use of a constitutive model that is capable of defining the flow stress as a function of temperature, strain, and strain rate. In this work, a material model for as-cast A356 is presented and applied in a range of fully coupled deformation models. Implicit and unscaled explicit models will be compared to explicit models with large amounts of scaling. Strategies for applying a material model to minimize error and maximize computational effort are discussed.

Introduction

Implicit finite element methods are well suited to modeling quasi-static thermomechanical processes such as casting because of the long durations and gradual changes in boundary conditions. However, dynamic processes with discontinuities in contact and large plastic deformation are better modeled employing an explicit approach. Explicit approaches rely on a direct calculation of dependent variables over a given time increment, whereas the implicit approach solves for dependent variables expressed in terms of coupled equations. Both involve numerical time integration to solve for the unknown workpiece displacements and temperatures, which is the basis for the resulting strains and stresses. A detailed comparison between the two solution techniques in terms of a thermomechanical framework has been outlined by Koric et al. [1].

The principal difference between implicit and explicit methods is that the implicit technique requires a matrix inversion to solve the system of equations that result from the problem, and the explicit solution does not. Furthermore, highly dynamic implicit models may experience convergence difficulties which may then lead to more iterations per increment and reduced increment size [2]. This results in explicit approaches being less computationally expensive and more robust in describing problems with contact as opposed to implicit models. This is in spite of explicit models requiring an order of magnitude more time steps to describe equivalent processes.

However, explicitly modelling dynamic processes with fine meshes occurring over long periods of time result in prohibitively long computation times. As a result, either the time of the process or the mass of the material is scaled to reduce the computation effort. To accommodate, the boundary conditions and material model must be modified. The penalty for scaling in this manner is inaccuracies in the inertial effects that evolve during deformation. The goal of the present work is to explore both strategies by comparing an experimental hot compression test conducted on as-cast A356. Simulations are constructed employing an experimentally derived material model, which is validated via isothermal implicit and explicit simulations in ABAQUS[1]. Explicit simulations with equal amounts of time and mass scaling are compared to an unscaled explicit model with thermal conditions applied. The computational gains as well as relative error in terms of simulated flow stress for each scaling factor are discussed.

Explicit coupled thermomechanical method

The present work has employed the commercial ABAQUS code, owed to the flexibility and capacity of the program to be customized. Additionally, ABAQUS provides both an implicit and explicit solver, allowing equivalent models to be simulated with either approach. The following describes the

[1]ABAQUS is a trademark of Dassault Systèmes, Surenes Cedex, France.

coupled explicit approach employed by this package to simulate a process with a time duration of t_p. The partial differential equation governing heat transfer is first integrated with a forward difference rule [3]:

$$T^N_{(t+\Delta t)} = T^N_t + \Delta t_{(t+\Delta t)} \left(C^N_t\right)^{-1} \left(P^N_t - F_t\right) \quad (1)$$

where T^N are nodal temperatures, C^N_t is the capacitance matrix, P^N_t is a nodal thermal load vector and F_t is the internal flux vector. Here, the subscript t refers to the time at the current increment with each increment being Δt long. The term $\left(C^N_t\right)^{-1} \left(P^N_t - F_t\right)$ is computed at the beginning of the increment at time t.

Next, the equations of motion are integrated using a central difference rule according to:

$$\ddot{u}_t = (M_t)^{-1}(P_t - I_t) \quad (2)$$

$$\dot{u}_{(t+\Delta t/2)} = \dot{u}_{(t-\Delta t/2)} + \frac{\Delta t_{(t+\Delta t)} + \Delta t_t}{2} \ddot{u}_t \quad (3)$$

$$u_{(t+\Delta t)} = u_t + \Delta t_{(t+\Delta t/2)} \dot{u}_{(t+\Delta t/2)} \quad (4)$$

Here, nodal displacements u are determined by integrating the accelerations at t via the mass matrix M and the difference between internal (I) and applied external (P) element forces. Eq. 3 shows how the velocity $\dot{u}$ is dependent on the time interval Δt, and therefore decides the stability of the overall solution.

Critical time increment Since acceleration is constant through Δt and a forward integration method is employed to solve for heat transfer, a coupled explicit scheme is conditionally stable; Δt must be smaller than the critical time step size dependent on the material and mesh according to:

$$\Delta t \leq \min\left(\frac{2}{\omega_{\max}}\left(\sqrt{1+\xi} - \xi\right), \frac{2}{\lambda_{\max}}\right) \quad (5)$$

where $\omega_{\max}$ is the highest frequency of the mechanical response and ξ is a fraction of critical damping in the highest mode and $\lambda_{\max}$ is the largest eigenvalue in the thermal solution response. On a per element basis, Δt can be estimated from a thermal and mechanical standpoint:

$$\Delta t \simeq \frac{(L_{\min})^2}{2\alpha}, \mathrm{L}_{\min}\left(\frac{E}{\rho}\right)^{-1/2} \quad (6)$$

where $L_{\min}$ is shortest distance across an element, α is the thermal diffusivity of the material, E is the modulus of elasticity and ρ the density of the material. Usually Δt is not limited thermally, but rather by the dilatational wave speed, which is approximated by $\sqrt{E/\rho}$. In actuality, the dilatational wave speed is a function of Poisson's ratio, elasticity, mass and the element dimensions. A more detailed stability analysis of explicit finite element methods has been conducted by Ling and Cherukuri [5]. However, for the present work, Eq. 5 and 6 demonstrate the principal deciding time factors for explicit analysis. Specifically, simulations with a duration of t_p with a fine mesh or extreme mesh distortion may require a large number of increments owing to a small Δt.

Abaqus/Explicit employs an adaptive method for determining time steps. Initially, time steps are calculated on a per-element basis, which is usually far less than the true stability limit for the entire domain. This time step is then updated based on a global estimation of the maximum frequency as the simulation proceeds and boundary conditions begin to take effect.

To decrease calculation times with an explicit method, it is necessary to either decrease the total simulated time or increase the time increment length. This is either accomplished through time or mass scaling, respectively, and the success of either method is dependant on the critical time step.

Time versus mass scaling While both strategies are equivalent in terms of reducing computational effort, time and mass scaling are quite different in their implementations. Mass scaling seeks to increase the length of time increments by scaling the material density by a factor f_m and thereby increasing Δt by decreasing the dilatational wave speed. Time scaling reduces computation time by applying loads faster than in actuality, decreasing the total simulated time. Both methods are proportional, where the time scaling factor $f_t = \sqrt{f_m}$. In a coupled framework, mass scaling requires the density of the material and dependent boundary conditions to be scaled. Time scaling requires that material rate sensitivities and thermal boundary conditions be amended. Depending on how the material model is implemented, time scaling is usually more difficult to implement for rate sensitive materials.

ABAQUS/Explicit allows for various implementations of mass scaling such that it is only applied to the mechanical solution and does not affect the thermal characteristics of the model. Although selective [6] and variable mass scaling techniques are possible, uniform mass scaling was employed. Here, Δt was specified directly and the solver increased ρ in all elements by the same amount to decrease the di-

latational wave speed.

Implementing a time scaling strategy is more complicated as it requires the rate dependency of the material, conductivity and thermal boundary conditions to be modified. The rate dependency is accommodated by directly scaling the strain rate in the constitutive behaviour. When applying time scaling to the thermal component, the Fourier and Biot (Fo and Bi) numbers must remain the same according to:

$$\text{Fo} = \frac{(Kf_t)(t_p/f_t)}{\rho C_p L^2} \qquad \text{Bi} = \frac{(hf_t)L}{kf_t} \tag{7}$$

where the process time t_p is scaled by f_t, accommodated by factoring the conductivity k and boundary heat transfer coefficients h to retain the same Biot number.

Model implementation and structure

As part of a concurrent study of the constitutive behaviour of as-cast A356, extensive compression testing at various elevated temperatures was conducted. This material characterization method has been modeled both to verify the implementation of a constitutive expression, in addition to providing a framework to investigate the effects of time and mass scaling. In the present work, this model is first employed to simulate a single experimental compression test, where baseline isothermal implicit and explicit solutions are used to validate the constitutive expression. The isothermal conditions were then replaced with transient thermal conditions had various degrees of time and mass scaling applied. This latter model formulation was used to establish the effects of time and mass scaling on a fully coupled explicit simulation.

Mechanical considerations

As shown schematically in Fig. 1, a 2-D axisymmetric model of a compression test specimen, nominally measuring 10 mm in diameter by 15 mm in length, was developed. The mesh consisted of 1200 square, four-noded, bi-linear, reduced integration elements (CAX4RT) with hourglass control and an initial element length L of 250 μm in each direction. The mechanical boundary conditions imposed for all models consisted of the following:

- Symmetry about the z axis representative of a cylindrical specimen geometry.

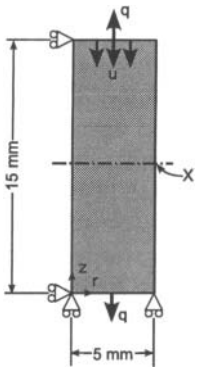

Figure 1: Schematic representation of the finite element model employed.

- Displacement of $u_z = 0$ at the base of the specimen corresponding to $z = 0$mm.
- A displacement of u corresponding to the experimental strain record at $z = 15$mm, implemented on a tabular basis.

Material properties

In order to capture the phenomenological simultaneous evolution of both strain hardening and strain rate effects with temperature for as-cast A356, a series of 55 compression tests spanning a large range of temperatures (30-500°C) and strain rates (~0.1-10 s^{-1}) were conducted. These compression tests were performed on specimens extracted from a wedge casting with a Gleeble[2] 3500 thermomechanical simulator fitted with isothermal anvils. During each test, the temperature and diametral deformation was measured at the center of the specimens. The yield point for each test was found with a 0.2% offset method employing temperature-corrected shear modulus [7], μ, to estimate the Young's modulus, E, according to:

$$\mu = 2.54 \times 10^4 \left(1 + \frac{300 - T}{2T_{\text{melt}}}\right) \quad \text{MPa} \tag{8}$$

$$E = 2\mu\,(1 + \nu) \quad \text{MPa} \tag{9}$$

based on pure aluminum, with T in Kelvin, $T_{\text{melt}} = 885.7$ K and $\nu = 0.33$. The expression for elasticity in Eq. 9 was implemented in the model on a tabular basis. The flow stress measured with these experiments was fit with an extended Ludwik-Hollomon [8] expression:

$$\sigma = K(T)\varepsilon^{N(T)} \left(\frac{\dot{\varepsilon}}{\dot{\varepsilon}_f}\right)^{M(T)} \tag{10}$$

[2]Gleeble is a trademark of Dynamic Systems, Inc., Poestenkill, NY.

where σ is the flow stress in MPa, ε is the equivalent strain, and $\dot{\varepsilon}$ is the equivalent strain rate. The normalization strain rate, $\dot{\varepsilon}_f$, is equal to 1 s^{-1} for mass-scaled simulations and equal to the time scaling factor f_t s^{-1} for time scaled simulations. The functions of temperature $K(T)$, $N(T)$ and $M(T)$ correspond to fitting constants for strength, strain hardening and strain-rate sensitivity, respectively. These functions were found through a Nedler-Mead technique from the experimental data such that:

$$K(T) = 8.12 \times 10^{-4}T^2 - 1.16T + 408 \quad (11)$$

$$N(T) = \begin{cases} -5.82 \times 10^{-4}T + 0.2 & T \leq 346 \\ -5.27 \times 10^{-3} & T > 346 \end{cases} \quad (12)$$

$$M(T) = 4.65 \times 10^{-11}T^{3.52} + 0.237 \quad (13)$$

with temperature T in °C. This constitutive behaviour was implemented in the model via the user subroutine UHARD for the implicit solution and VUHARD for explicit cases.

Density was taken to be $\rho = 2670$ kg/m^3, and the coefficient of thermal expansion, specific heat and conductivity, α, C_p and K, respectively, were implemented in a tabular fashion according to Hétu et al. [9]:

$$\alpha(T) = 2.26 \times 10^7 + 2.39 \times 10^{-8}T \quad °C^{-1} \quad (14)$$

$$C_p(T) = 0.427T + 898.72 \quad J/kg°C \quad (15)$$

$$k(T) = 4.15T + 7146 \quad W/m°C \quad (16)$$

All material properties and constitutive behaviour were assumed to be isotropic.

Validation simulations

In order to validate the implementation of the material model and the mechanical boundary conditions, implicit and unscaled explicit simulations were conducted without considering heat transfer (i.e. isothermal). This was compared against flow stress from a compression test with an average temperature of 202.8°C and $\dot{\varepsilon} = 8.25 s^{-1}$.

For these simulations, the experimental temperature record was directly assigned to all nodes, in the same manner as u. In order to directly compare the simulation to experimental results, strain was extracted from the nodal displacement record at X in Fig. 1. The average von Mises stress in elements immediately below centerline at point X ($z = 7.5$ mm) was also extracted. These simulations showed that there is no difference between unscaled explicit and implicit solutions at X. Furthermore, there is good agreement with the experimental flow stress, characterized by a low (< 2%) mean square error.

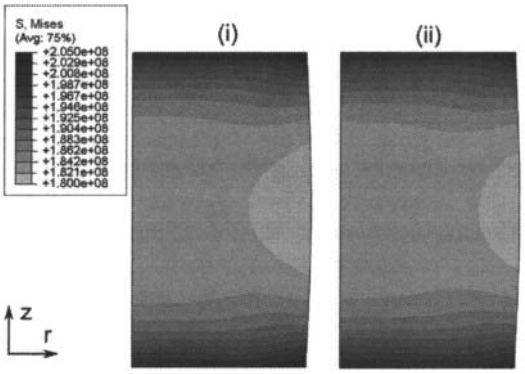

Figure 2: Simulated final von Mises stress state in Pa for baseline (i) implicit versus (ii) explicit models.

Thermal conditions for scaled models

In order to assess both the mechanical and thermal aspects of time and mass scaled models, thermal boundary conditions were imposed to approximate heat evolution in the experimental test. Heat due to inelastic deformation was generated corresponding to a constant inelastic heat fraction of $\beta = 0.9$. This was countered with a flux $q = h(T - T_\infty)$ applied at $z = 0$ and $z = 15$ mm (Fig. 1), with $h = 4 \times 10^3$ W/m^2°C and a constant $T_\infty = 180$°C. This flux represents the heat transfer to the Gleeble isothermal anvils.

Both this flux and inelastic heat generation were explicitly implemented without scaling and the flow stresses at point X (Fig. 1) were found to be identical to the implicit values as demonstrated in Fig. 2. Globally, the distribution of stress is nearly identical being within 2 MPa at all points. As a result, an unscaled explicit simulation has been used as a baseline to evaluate the effects of time scaling and mass scaling.

Effects of scaling

The baseline explicit model described above was time scaled by f_t equal to 10, 25, 50 and 100. These simulations were compared to models with equivalent amounts of mass scaling applied. As the flow stress is a direct function of temperature, this has been used as the principal metric to compare the ability of each simulation to track the evolution of stress, strain and temperature. Any variation in temperature or strain results in a significant variation in the flow stress. A comparison between predicted flow stresses is provided in Fig. 3.

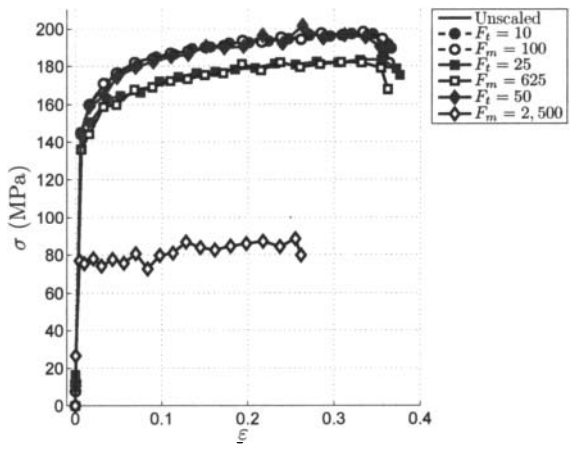

Figure 3: Predicted flow stresses for time and mass scaling.

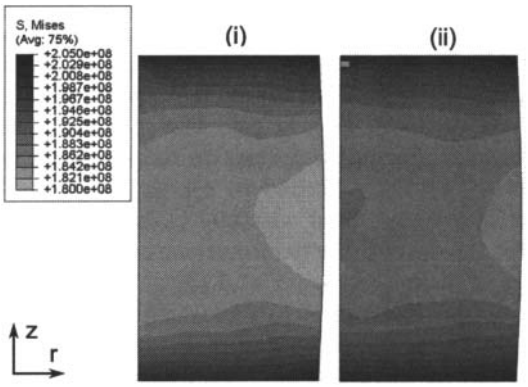

Figure 4: Simulated final von Mises stress state in Pa for the model time scaled by $f_t = 10$ in (i) as compared to an equivalent mass scaling $f_m = 100$ in (ii).

Both mass and time scaling strategies result in significantly shortened computation times. This has been quantified with a speed up factor, C, which is defined as the ratio of unscaled simulation computation time to scaled simulation computation time. Table 1 provides C for each simulation type and clearly demonstrates the large improvements made. The $f_t = 10$ simulation ran 7.1 times faster and the $f_m = 100$ simulation ran 8.86 times faster than the baseline unscaled simulation. Beyond this scaling point, C did not increase as much for mass as compared to time scaling owing to more time increments caused by solution instability. However, if the simulation corresponding to $f_t = 10$ is considered to be at the limit of numerically stability, then mass scaling does provide a 20% improvement in computation time.

Table 1: Simulation execution time speed up factor C for time and mass scaling

f_t	C	f_m	C
10	7.10	100	8.86
25	17.72	625	12.00
50	44.29	2500	24.01
100	95.15	10000	46.71

Stability

Both time and mass scaling provide a reasonably accurate simulated flow stress at $f_t = 10$ and $f_m = 100$ as compared to the unscaled process. However, when compared of the von Mises stress contours of the unscaled version (Fig. 2), the time scaled version is closer than that of the mass scaled (Fig. 4). Furthermore, a single element has locked, meaning it is exhibiting numerical instability. This locked element has in turn affected the stress distribution. This is likely because the domain is sensitive to instability at this location, as this is where the largest temperature and stress gradients occur. At greater scaling factors, significant deviations both globally and locally at the midplane X are apparent. At $f_t = 25$ and $f_m = 625$, both simulations show low flow stresses relative to the unscaled simulation with marginally more strain. This demonstrates that the simulation is unstable as there is evidence of non-uniform deformation. At $f_t = 50$ and $f_m = 2500$, there is a significant difference between the time and mass scaled versions: the time scaled flow stress matches the unscaled version, while the mass scaled flow stress severely underestimates the unscaled version. Globally, the von Mises stress for both scaling techniques do not match stress and deformation distribution seen in the unscaled version.

Both models show evidence of element locking, with the time scaled version showing only a few locked elements in the most sensitive portion of the domain. The extent of element locking in the mass scaled version is on a much larger scale, with only a few elements in the center of the model remaining unlocked. Both the time and mass scaled simulations have diverged and are unstable with scaling at this level.

Inertial effects of scaling

The main source of inaccuracy by scaling is due to the development of inertial effects. These are characterized by the evolution of increased kinetic energy.

Sudden increases in kinetic energy are usually countered by the small amount of damping (Eq. 5) which was equivalent in all of the explicit simulations in the present work. A general guideline to avoid instability *a priori* for bulk deformation models is to impose deformation rates limited to 1% of the dilatational wave speed [4]. Even with the highest time scaling factor ($t_f = 100$), the deformation speed was kept an order of magnitude lower at 0.1% of the wave speed. An alternative approach is to ensure that the total kinetic energy is an order of magnitude lower or less than the internal energy (strain energy) during the course of a simulation.

The largest input of kinetic energy to the model is the initial elastic loading. As the deformation wave plasticizes the material, the bulk of this kinetic energy is translated to strain energy. In the unscaled simulation, the average percentage of strain energy attributed to kinetic energy prior to yield, $K_U = 0.14\%$. Scaling factors increase this by many orders of magnitude, as well as increasing the duration prior to yield that kinetic energy is more than 5% of the strain energy. Furthermore, there is evidence of discontinuities as the scaling factor increases, and the simulations become more unstable. A measure of how the kinetic energy ratio is multiplied by scaling prior to yield is given by $K_R = |K_S/K_U|$ in Table 2, where K_S is the kinetic energy ratio for scaled simulations and K_U unscaled. K_S is significantly higher for time scaled simulations as opposed to the mass scaled versions, owing to larger peak kinetic energy at the start of the deformation, however declines at approximately the same rate as the equivalent mass scaled version.

Table 2: Average increase in kinetic energy ratio prior to yield

f_t	K_R	f_m	K_R
10	173.1	100	92.8
25	468.4	625	350.5
50	1243.1	2500	832.8

Summary

A constitutive material model has been implemented in ABAQUS and has been validated both implicitly and explicitly by specifying exact thermal conditions at all nodes. From this isothermal model, the explicit implementation was extended to include thermal considerations encompassing unequal rates of heat generation due to inelastic deformation and conduction. This baseline model was then used as a metric to compare both time and mass scaling strategies. The simulation results were compared based on both flow stress locally as well as globally.

Both time and mass scaling provide reasonable solutions as compared to the baseline model up to factors of $f_t = 10$ and $f_m = 100$. At these scaling factors, time scaling provided a better match to unscaled simulations. With increasing scaling factors, the model provided increasingly unstable results, predominantly in the numerically sensitive areas of the domain. Mass scaling with equivalent time scaling factors was found to provide more unstable results with a higher computational penalty owing to non-uniform mesh distortion as compared to time scaling. This is in spite of less kinetic energy being imparted to the model through scaling with mass as opposed to time.

In comparing equivalent uniform scaling strategies, even though time scaling necessitates scaling both mechanical and thermal boundary conditions, it has been found to be the best overall strategy to reduce computational time. However, if the scaling factor at which model instability is known, mass scaling is computationally advantageous.

References

[1] S. Koric, L. C. Hibbeler, B. G. Thomas, Int. J. Numer. Methods Eng. 78 (2009) 1-31.

[2] A. M. Prior, J. Mater. Process. Technol. 45 (1994) 649-656.

[3] ABAQUS Inc., ABAQUS Users Manual (version 6.10). Dassault Systèmes Simulia Corp, 2010.

[4] H. Schmidt, J. Hattel, Modelling Simul. Mater. Sci. Eng. 13 (2005) 77-93.

[5] X. Ling, H. P. Cherukuri, Comput. Mech. 29 (2002) 430-440.

[6] L. Olovsson, K. Simonsson, Commun. Numer. Meth. Engng 22 (2006) 77-82.

[7] H.J. Frost, M.F. Ashby, Deformation-Mechanism Maps: The Plasticity and Creep of Metals and Ceramics, Pergamon Press, 1982.

[8] J.-M. Drezet, A.B. Phillion, Metall. Mater. Trans. A 41A (2010) 3396-3404.

[9] J.-F. Hétu, D.M. Gao, K.K. Kabanemi, S. Bergeron, K.T. Nguyen, C.A. Loong, Adv. Perform. Mater. 5 (1998) 6582.